Void coalescence in porous ductile solids containing two populations of cavities

Léo Morin[a,*], Jean-Claude Michel[b]

[a] *Laboratoire PIMM, Ensam, CNRS, Cnam, HESAM Université, UMR 8006, 151 boulevard de l'Hopital, 75013 Paris, France*
[b] *Laboratoire de Mécanique et d'Acoustique, Aix-Marseille Univ, CNRS, Centrale Marseille, UMR 7031, 4 impasse Nikola Tesla, CS 40006, 13453 Marseille Cedex 13, France*

ABSTRACT

A model of coalescence by internal necking of primary voids is developed which accounts for the presence of a second population of cavities. The derivation is based on a limit-analysis of a cylindrical cell containing a mesoscopic void and subjected to boundary conditions describing the kinematics of coalescence. The second population is accounted locally in the matrix surrounding the mesoscopic void through the microscopic potential of Michel and Suquet (1992) for spherical voids. The macroscopic criterion obtained is assessed through comparison of its predictions with the results of micromechanical finite element simulations on the same cell. A good agreement between model predictions and numerical results is found on the limit-load promoting coalescence.

1. Introduction

Ductile failure is one of the most dominant mode of failure of metallic alloys at room temperature. It is well recognized that failure is essentially controlled by the nucleation, growth and coalescence of *primary* voids (Benzerga and Leblond, 2010; Benzerga et al., 2016; Pineau et al., 2016). Those primary voids usually nucleate on large inclusions by particle cracking or interface decohesion, and then grow by diffuse plastic deformation without notable interactions with neighboring cavities. When the onset of coalescence is reached, plastic deformation becomes localized between neighboring primary voids, which accelerates the failure mechanism leading ultimately to the final fracture. It has been shown that the nucleation and growth of *secondary* voids in aluminum alloys and in steels quicken the damage process of primary voids and thus lead to a reduction of ductility (Cox and Low, 1974; Marini et al., 1985; Perrin and Leblond, 1990; Fabregue and Pardoen, 2008). Those secondary voids nucleate in general on much smaller particles and thus are at least one order of magnitude smaller than primary voids.

The modeling of ductile fracture has first focused on the role played by the *primary voids* in the growth phase where plasticity is diffuse, with the pioneering contribution of Gurson (1977). This model, based on the limit-analysis of a spherical cell containing a spherical void and made of a von Mises material, has permitted to describe accurately the effective behavior of porous materials for high values of the stress triaxiality (Tvergaard and Needleman, 1984). Due to its intrinsic limitations, this

growth model has been widely extended to account for more realistic microstructures, notably through ellipsoidal voids (Gologanu et al., 1993; Madou and Leblond, 2012), plastic anisotropy of the matrix (Monchiet et al., 2008; Keralavarma and Benzerga, 2010; Morin et al., 2015b) and strain hardening effects (Leblond et al., 1995; Morin et al., 2017). Another framework, based on non-linear homogenization (Ponte Castaneda, 1991; Willis, 1991), has also been developed to derive micromechanical void growth models for spherical (Michel and Suquet, 1992) and ellipsoidal (Kailasam and Ponte Castaneda, 1998; Danas and Ponte Castaneda, 2009) cavities. The modeling of void growth has then been followed by the modeling of coalescence of primary voids where plasticity is this time localized. It started with the contribution of Thomason (1985) who derived a semi-analytical model providing the limit-load of coalescence of primary voids. It was then revisited by the determinant work of Benzerga and Leblond (2014) providing the first micromechanical model of void coalescence, and followed by extensions accounting for more realistic situations (Morin et al., 2015a, 2016; Torki et al., 2015, 2017; Hure and Barrioz, 2016; Keralavarma and Chockalingam, 2016; Keralavarma, 2017; Gallican and Hure, 2017).

If the importance of *secondary voids* on ductile failure is well recognized, its modeling, on the other hand, has only been the focus of a few studies. Most of the efforts have focused on the influence of a second population on void growth, after the initial work of Perrin and Leblond (1990, 2000) based on the limit-analysis of a hollow sphere (modeling primary voids) made of a Gurson model in the matrix

(modeling secondary voids). Their model, restricted to hydrostatic loadings, has been extended to triaxial loadings with different approaches. Vincent et al. (2009a, b); Julien et al. (2011); Vincent et al. (2014a, b) provided estimates of the macroscopic yield criterion using a proper combination of limit-analysis and variational homogenization techniques, while Shen et al. (2012, 2017) performed a limit-analysis of a hollow sphere made of an elliptic (compressible) criterion of Green type. In both works, the presence of the second population of cavities lead to a reduction of ductility. The observations made in those analytical works have been completed by numerical micromechanical simulations (Faleskog and Shih, 1997; Fabregue and Pardoen, 2008; Khdir et al., 2014; Zybell et al., 2014; Khan and Bhasin, 2017; Boittin et al., 2017), emphasizing that the second population of cavities plays mostly a role on the phenomenon of coalescence of primary voids: the onset of coalescence occurs more quickly and the degradation of the ligament between neighboring primary voids is accelerated by the presence of a second population. Those observations have motivated the development of coalescence models accounting for secondary voids, based on phenomenological extensions of Thomason (1985)'s criterion calibrated with numerical micromechanical simulations (Fabregue and Pardoen, 2008, 2009; Tekoglu, 2015).

The presence of secondary voids appears to be determinant in the coalescence of primary voids in many metallic alloys and thus is expected to play an important role on the final stage of failure of ductile materials. The modeling of this effect is restricted to phenomenological extensions of classical coalescence models which naturally calls for a rigorous micromechanical analysis. The development of a micromechanical model of coalescence incorporating the effect of a secondary population of voids thus seems of interest to reproduce accurately the final stage of failure of many metallic alloys. The aim of this work is to develop such a model. The paper is organized as follows:

- Section 2 presents the problem considered and notably the theoretical approach of limit-analysis in the case of Green materials.
- Section 3 is devoted to the derivation of the model of coalescence accounting for the presence of secondary voids.
- Section 4 compares the predictions of the theoretical model with the results of finite element simulations for the limit-load of coalescence.
- Finally, Section 5 studies the influence of the plastic porous model considered in the matrix and compares the proposed model with the existing model of Fabregue and Pardoen (2008).

2. Position of the problem

2.1. Preliminaries

We are interested in the modeling of ductile porous solids containing two populations of cavities of separate size. A typical example of double porous solids is irradiated uranium dioxide (UO_2), represented in Fig. 1 (a). When irradiated, its microstructure shows two populations of cavities, spherical cavities at the smallest scale (microscopic scale) and spheroidal cavities at the larger scale (mesoscopic scale). When the deformation localizes, coalescence of primary voids is observed, promoted by the presence of secondary voids. In order to describe the influence of the secondary voids on the coalescence of primary ones, the strategy adopted in this work is to consider a periodic arrangement of primary voids subjected to boundary conditions mimicking the kinematics of coalescence. Since our objective is to derive an analytical model, it is not reasonable to consider a complete description of secondary voids as shown in Fig. 1(b). Thus, secondary voids are accounted for through a homogenized model of plastic porous materials, in the matrix surrounding the primary void (see Fig. 1(c)). We are then looking for the overall behavior of primary voids embedded in some compressible material and subjected to boundary conditions of coalescence type. We assume that secondary voids will not grow

significantly so no localization between them is allowed. This assumption is supported by the simulations of Zybell et al. (2014) emphasizing that secondary voids promote coalescence of primary voids without any microscopic localization. Thus, coalescence between secondary voids is disregarded in the present work so they will be modeled using a homogenized model accounting solely for void growth.

2.1.1. Geometry

The elementary cell considered to derive the coalescence criterion is, following Benzerga and Leblond (2014), a cylindrical cell Ω containing a cylindrical void ω (Fig. 2). The cylindrical geometry is characterized by dimensionless parameters (Benzerga and Leblond, 2014; Morin et al., 2016): the *void aspect ratio* $W \equiv h/R$, the *ligament parameter* $\chi \equiv R/L$ and the *cell aspect ratio* $\lambda \equiv H/L$. A fourth, useful parameter related to the first three is the *volume fraction of the voided band* $c = h/H = W\chi/\lambda$. The local orthonormal basis associated with the cylindrical coordinates r, θ, z is denoted $(\mathbf{e}_r, \mathbf{e}_\theta, \mathbf{e}_z)$ and that associated with the Cartesian coordinates x_1, x_2, x_3 is denoted $(\mathbf{e}_1, \mathbf{e}_2, \mathbf{e}_3)$, with $\mathbf{e}_3 = \mathbf{e}_z$.

Coalescence is supposed to occur in the plane $\mathbf{e}_1$–$\mathbf{e}_2$, due to a major applied stress parallel to the axis $\mathbf{e}_3$. Coalescence starts when the strain rate localizes in the horizontal ligament between neighboring voids (Koplik and Needleman, 1988). The cell is then divided into two parts, the central one Ω_{lig} containing the plastic horizontal inter-void ligament and the void ω, and the rigid regions above and below the void denoted $\Omega - \Omega_{\text{lig}}$ (see Fig. 2).

2.1.2. Boundary conditions

The cell is subjected to boundary conditions of the form

$$\begin{cases} v_r(r = L, z) &= \quad 0, \quad -H \leq z \leq H, \\ v_z(r, z = \pm H) &= \pm D_{33}H, \quad 0 \leq r \leq L. \end{cases} \tag{1}$$

The cylindrical shape of the cell and the quasi-periodic boundary conditions considered are an approximation of elementary cell in a periodic material in a coalescence regime (see Koplik and Needleman (1988), Morin et al. (2015a)).

2.1.3. Material

In order to account for a secondary void population, we consider that the plastic horizontal inter-void ligament obeys Green's criterion

$$\varphi(\boldsymbol{\sigma}) = N\sigma_{\text{eq}}^2 + \frac{9}{2}M\sigma_{\text{m}}^2 - \sigma_0^2 = 0, \qquad \forall \, \mathbf{x} \in \Omega_{\text{lig}} - \omega, \tag{2}$$

where σ_0 is the yield stress. This type of criterion, which accounts for the material compressibility through the material parameters N and M, has been previously considered to derive macroscopic models for the growth of primary voids (Shen et al., 2012, 2017). Here, we consider Michel and Suquet (1992)'s potential for plastic porous solids which corresponds to the particular case

$$M = \frac{1}{2(\ln(f_s))^2} \quad ; \quad N = \frac{1 + 2f_s/3}{(1 - f_s)^2}, \tag{3}$$

where f_s denotes the volume fraction of the second population. It should be noted that f_s can reach high values and can even be greater than the porosity of the primary void as long as there is no interaction between secondary voids to avoid their coalescence. In practice, it is likely that secondary voids will coalesce if f_s is roughly higher than 10^{-1}; this choice is quite arbitrary since coalescence does not depend on the porosity but on the distribution of cavities (Thomason, 1985; Benzerga and Leblond, 2010). Thus, as a first approximation, it is reasonable to consider that the present analysis is valid if $0 \leq f_s \leq 10^{-1}$. Michel and Suquet (1992)'s criterion has been chosen over Gurson (1977)'s classical model for porous materials because the integration of the local plastic potential (in the derivation of the macroscopic criterion) will be incontestably easier with an elliptic criterion. The consequences of this
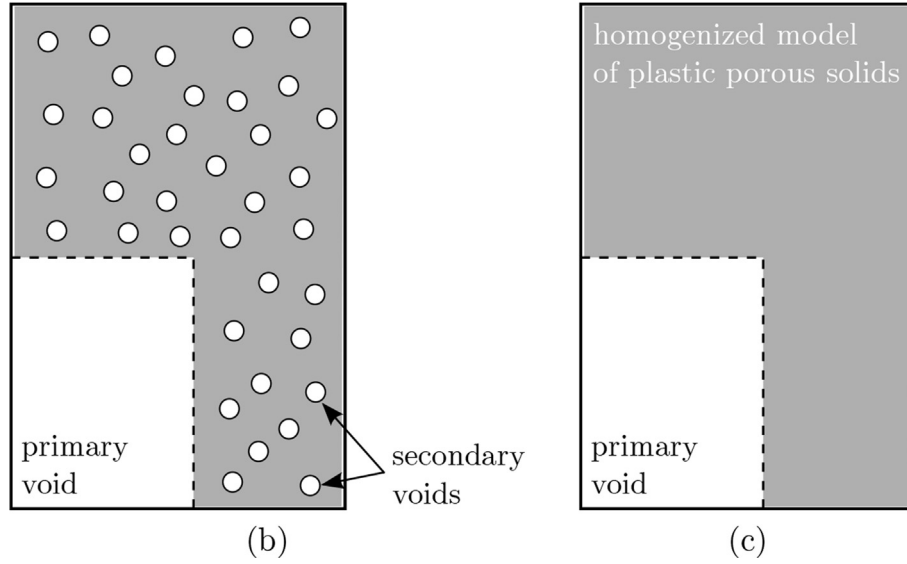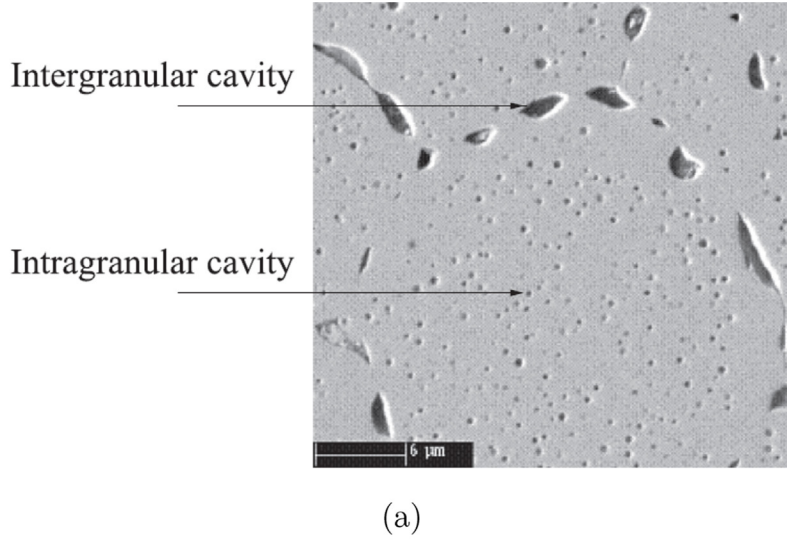
Fig. 1. Scale transition approach for the modeling of double porous materials in the coalescence phase. (a) Example of a double porous material (micrography of irradiated UO_2 after Dubourg et al. (2005)). (b) "Discrete" cell model accounting explicitly for the second population of voids. (c) "Homogenized" cell model accounting for the second population of voids through an homogenized model of plastic porous solids.

choice are discussed in Section 5.1.

2.2. Principles of limit-analysis

The macroscopic yield locus of the double porous material can be determined using the upper-bound theorem of limit-analysis (see e.g. Leblond et al. (2018)); it is described by the parametric equation

$$\mathbf{\Sigma} = \frac{\partial \Pi}{\partial \mathbf{D}}(\mathbf{D}), \tag{4}$$

where the macroscopic stress and strain rate tensors $\mathbf{\Sigma}$ and $\mathbf{D}$ are defined as the volume averages of their microscopic counterparts $\boldsymbol{\sigma}$ and $\mathbf{d}$. The macroscopic plastic dissipation $\Pi(\mathbf{D})$ in equation (4) is defined here by:

$$\Pi(\mathbf{D}) = \inf_{\mathbf{v} \in \mathcal{K}(\mathbf{D})} (1 - c\chi^2)\langle \pi(\mathbf{d})\rangle_{\Omega-\omega}, \tag{5}$$

where the set $\mathcal{K}(\mathbf{D})$ consists of velocity fields $\mathbf{v}$ kinematically admissible with $\mathbf{D}$ and where the notation $\langle . \rangle_{\Omega-\omega}$ stands for volume averaging over the volume $\Omega - \omega$. In the case of a Green material obeying criterion (2), the microscopic plastic dissipation $\pi(\mathbf{d})$ reads

(Shen et al., 2012)

$$\pi(\mathbf{d}) = \sigma_0 \sqrt{2\frac{d_m^2}{M} + \frac{d_{eq}^2}{N}}, \tag{6}$$

where d_{eq} is the von Mises equivalent strain rate and d_m the mean strain rate, both associated with the velocity field $\mathbf{v}$ and defined by

$$d_{eq} = \sqrt{\frac{2}{3}\mathbf{d}' : \mathbf{d}'}, \qquad \mathbf{d}' = \mathbf{d} - d_m\mathbf{I}, \qquad d_m = \frac{1}{3}\text{tr}\mathbf{d}. \tag{7}$$

3. A macroscopic criterion for void coalescence in plastic solids containing two populations of cavities

3.1. Trial velocity field

The trial velocity field we are looking for must be *compressible* and should verify two properties:

1. When the porosity of the second population becomes zero, that is when the matrix obeys incompressible von Mises criterion (*i.e.*
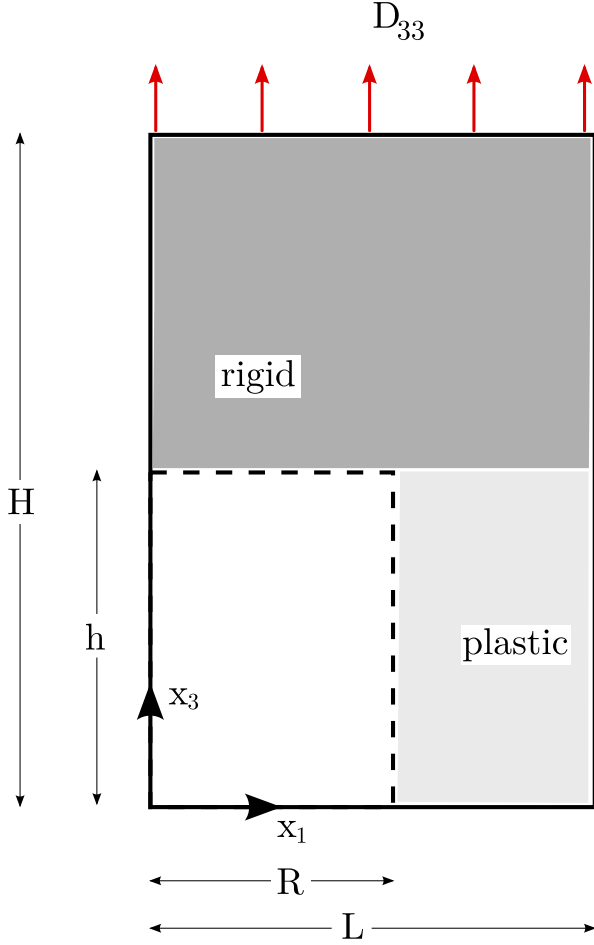
Fig. 2. Geometry of the problem.

$f_s = 0$, $M = 0$ and $N = 1$), the velocity field should verify the property of incompressibility (see Benzerga and Leblond (2014); Morin et al. (2015a); Hure and Barrioz (2016) for existing incompressible velocity fields).

2. When there is no primary void but only secondary voids, the problem reduces to a full cylinder made of a Green material subjected to uniaxial tension. In this case, the cylinder can deform in contrast with the incompressible case. The most simple assumption to describe this kinematic consists in a linear axial velocity field.

The full velocity field proposed consists in some interpolation of the two fields just expounded and is taken to be of the form

$$\begin{cases} v_r(r, z) = (1 - \alpha)v_r^{\text{inc}}(r, z), \\ v_z(z) = (1 - \alpha)v_z^{\text{inc}}(z) + \beta D_{33} z, \end{cases} \quad (8)$$

where $\mathbf{v}^{\text{inc}}$ denotes an "incompressible" field describing the kinematic of coalescence for a von Mises material, α and β parameters accounting for the compressibility and the term $D_{33} z$ corresponds to the deformation of the full compressible cylinder.

The parameters α and β are necessarily linked by boundary conditions (in $z = h$)

$$(1 - \alpha)D_{33}H + \beta D_{33}h = D_{33}H, \quad (9)$$

which leads to $\beta = \frac{\alpha}{c}$. Consequently, the velocity field for the coalescence of a double porous material reads

$$\begin{cases} v_r(r, z) = (1 - \alpha)v_r^{\text{inc}}(r, z), \\ v_z(z) = (1 - \alpha)v_z^{\text{inc}}(z) + \frac{\alpha}{c}D_{33}z. \end{cases} \quad (10)$$

The parameter α, which permits to account for the compressibility, plays the same role as the parameter A of Vincent et al. (2009a); Shen et al. (2012). It should be noted that the value of the parameter α is not known at this stage and will be classically determined in order to minimize the macroscopic plastic dissipation.

Regarding the choice of the "incompressible" velocity field, it has been shown in Morin et al. (2015a) that a good candidate is the so-called "continuous velocity field", which is very close to the exact velocity field calculated numerically in a large range of geometric parameters. Therefore, we will consider in this work that the incompressible velocity field is given by

$$\begin{cases} v_r^{\text{inc}}(r, z) = \frac{H}{h^2}D_{33}(h - z)\left(\frac{L^2}{r} - r\right), \\ v_z^{\text{inc}}(z) = 2\frac{H}{h^2}D_{33}\left(hz - \frac{z^2}{2}\right). \end{cases} \quad (11)$$

3.2. Strain rate and microscopic plastic dissipation

The non-zero components of the strain rate associated to the velocity field defined by equations (10) and (11) read

$$d_{rr} \equiv \frac{\partial v_r}{\partial r} = (1 - \alpha)d_{rr}^{\text{inc}}, \quad d_{\theta\theta} \equiv \frac{v_r}{r} = (1 - \alpha)d_{\theta\theta}^{\text{inc}}, \quad d_{zz} \equiv \frac{\partial v_z}{\partial z}$$

$$= (1 - \alpha)d_{zz}^{\text{inc}} + \frac{\alpha}{c}D_{33}, \quad d_{rz} \equiv \frac{1}{2}\frac{\partial v_r}{\partial z} = (1 - \alpha)d_{rz}^{\text{inc}},$$

where the components of the "incompressible" strain rate tensor are given by

$$d_{rr}^{inc} = \frac{H}{h^2}D_{33}(h - z)\left(\frac{-L^2}{r^2} - 1\right), \quad d_{\theta\theta}^{inc} = \frac{H}{h^2}D_{33}(h - z)\left(\frac{L^2}{r^2} - 1\right), \quad d_{zz}^{inc}$$

$$= 2\frac{H}{h^2}D_{33}(h - z), \quad d_{rz}^{inc} = -\frac{H}{2h^2}D_{33}\left(\frac{L^2}{r} - r\right).$$

In order to calculate the microscopic plastic dissipation defined by equation (6), we need the expressions of the mean and equivalent strain rate. The mean strain rate is directly given by

$$d_{\text{m}} = \frac{\alpha D_{33}}{3c}. \quad (12)$$

It is interesting to note that the mean strain rate is uniform in the ligament and depends on the parameter α. In particular the value $\alpha = 0$ leads to $d_{\text{m}} = 0$ which is consistent with the fact that the velocity field reduces in this case to the "incompressible" velocity field of Morin et al. (2015a).

Let us derive now the equivalent strain rate. First, the deviatoric part $\mathbf{d}'$ of the strain rate $\mathbf{d}$ reads

$$\begin{cases} d_{rr}' = (1 - \alpha)d_{rr}^{\text{inc}} - \frac{\alpha D_{33}}{3c}, \quad d_{\theta\theta}' = (1 - \alpha)d_{\theta\theta}^{\text{inc}} - \frac{\alpha D_{33}}{3c}, \\ d_{zz}' = (1 - \alpha)d_{zz}^{\text{inc}} + \frac{2\alpha D_{33}}{3c}, \quad d_{rz}' = (1 - \alpha)d_{rz}^{\text{inc}}. \end{cases}$$

The square of the equivalent strain rate thus reads

$$d_{\text{eq}}^2 = \frac{2}{3}(d_{rr}'^2 + d_{\theta\theta}'^2 + d_{zz}'^2 + 2d_{rz}'^2) = (1 - \alpha)^2(d_{\text{eq}}^{\text{inc}})^2 + \frac{4(1 - \alpha)\alpha}{3c}D_{33}d_{zz}^{\text{inc}}$$

$$+ \frac{4}{9}\left(\frac{\alpha}{c}\right)^2 D_{33}^2, \quad (13)$$

where the expression of the "incompressible" equivalent strain rate $d_{\text{eq}}^{\text{inc}}$ is given by

$$(d_{\text{eq}}^{\text{inc}})^2 = \frac{H^2}{3h^4}D_{33}^2\left[4(h - z)^2\left(\frac{L^4}{r^4} + 3\right) + \left(\frac{L^2}{r} - r\right)^2\right]. \quad (14)$$

We thus have

$$d_{\text{eq}}^2 = \left((1-\alpha)^2 \frac{H^2}{3h^4} \left[4(h-z)^2 \left(\frac{L^4}{r^4} + 3 \right) + \left(\frac{L^2}{r} - r \right)^2 \right] \right.$$
$$\left. + \frac{\alpha}{c}(1-\alpha)\frac{8H}{3h^2}(h-z) + \frac{4}{9}\left(\frac{\alpha}{c}\right)^2 \right) D_{33}^2. \tag{15}$$

The microscopic plastic dissipation consequently reads

$$\pi(d) = \sigma_0 D_{33} \left\{ \left(\frac{4}{9N} + \frac{2}{9M} \right)\left(\frac{\alpha}{c}\right)^2 + \frac{(1-\alpha)^2}{N}\frac{H^2}{3h^4}\left[4(h-z)^2 \times \left(\frac{L^4}{r^4} + 3\right) \right. \right.$$
$$\left. \left. + \left(\frac{L^2}{r} - r\right)^2 \right] + \frac{\alpha(1-\alpha)}{cN}\frac{8H}{3h^2}(h-z) \right\}^{1/2}. \tag{16}$$

3.3. Macroscopic plastic dissipation

The microscopic plastic dissipation (16) obtained for the velocity field (10) is now integrated in order to provide an upper estimate $\Pi^+(\mathbf{D})$ of the macroscopic plastic dissipation $\Pi(\mathbf{D})$ defined by equation (5). In the following, the upper indice $+$ will be omitted for conciseness. The upper estimate of the macroscopic plastic dissipation thus reads

$$\Pi(D) = \frac{1}{\text{vol}(\Omega)} \int_{\Omega_{\text{lig}-\omega}} \pi(d)\mathrm{d}\Omega,$$
$$= \frac{\sigma_0 D_{33}}{\text{vol}(\Omega)} \int_R^L \int_0^h \left\{ \left(\frac{4}{9N} + \frac{2}{9M} \right)\left(\frac{\alpha}{c}\right)^2 + \frac{(1-\alpha)^2}{N}\frac{H^2}{3h^4}\left[4(h-z)^2 \right. \right.$$
$$\left. \left. \times \left(\frac{L^4}{r^4} + 3\right) + \left(\frac{L^2}{r} - r\right)^2 \right] + \frac{\alpha(1-\alpha)}{cN}\frac{8H}{3h^2}(h-z) \right\}^{1/2} 4\pi r \mathrm{d}r\mathrm{d}z. \tag{17}$$

After the change of variables $u = r^2/L^2$ and $v = (h-z)/L$ and some calculations, the macroscopic plastic dissipation reads

$$\Pi(\mathbf{D}) = \frac{\sigma_0 D_{33}}{W\chi} \int_{\chi^2}^1 \int_0^{W\chi} \left\{ \left(\frac{4}{9N} + \frac{2}{9M} \right)\alpha^2 + \frac{(1-\alpha)^2}{3N(W\chi)^2}\left[\frac{(1-u)^2}{u} \right. \right.$$
$$\left. \left. + 4\frac{(1+3u^2)}{u^2}v^2 \right] + \frac{8\alpha(1-\alpha)}{3NW\chi}v \right\}^{1/2} \mathrm{d}u\mathrm{d}v. \tag{18}$$

The macroscopic plastic dissipation (18) involves a double integral but this should not be a real issue since it may be easily evaluated numerically with a reasonable number of integration points. It is worth noting that the integration over the variable v can be performed analytically by using the following relation

$$\int \sqrt{1 + Av + Bv^2}\,\mathrm{d}v = \frac{(A + 2Bv)\sqrt{Av + Bv^2 + 1}}{4B}$$
$$- \frac{(A^2 - 4B)\log(2\sqrt{B}\sqrt{Av + Bv^2 + 1} + A + 2Bv)}{8B^{3/2}}, \tag{19}$$

at the expense of a less user-friendly model.

3.4. Effective macroscopic criterion

First, we need to determine the value of α. The optimal parameter, denoted α_{opt}, is that minimizing the macroscopic plastic dissipation. Thus, it verifies

$$\frac{\partial \Pi}{\partial \alpha}(\alpha_{\text{opt}}) = 0. \tag{20}$$

In practice, the parameter α_{opt} can be determined numerically. Tabulated values for a great number of geometrical parameters χ and W and various porosities f_s are given in Appendix A.

Then, the macroscopic criterion is expressed as the macroscopic axial stress Σ_{33} promoting plastic flow given by

$$\Sigma_{33} = \frac{\partial \Pi}{\partial D_{33}} = \frac{\Pi}{D_{33}}. \tag{21}$$

The semi-analytical expression of the macroscopic yield criterion therefore finally reads

$$\Phi(\mathbf{\Sigma}; \chi, W, f_s) = \frac{|\Sigma_{33}|}{\sigma_0} - \frac{1}{W\chi} \int_{\chi^2}^1 \int_0^{W\chi} \left\{ \left(\frac{4}{9N} + \frac{2}{9M} \right)\alpha_{\text{opt}}^2 \right.$$
$$+ \frac{(1-\alpha_{\text{opt}})^2}{3N(W\chi)^2}\left[\frac{(1-u)^2}{u} \right.$$
$$\left. \left. + 4\frac{1 + 3u^2}{u^2}v^2 \right] + \frac{8\alpha_{\text{opt}}(1-\alpha_{\text{opt}})}{3NW\chi}v \right\}^{1/2} \mathrm{d}u\mathrm{d}v \leq 0. \tag{22}$$

3.5. Evolution equations of internal parameters

In order to get a full model of plasticity, it is necessary to complete the yield criterion by evolution equations of internal parameters. This corresponds to the microstructural parameters defining primary voids (χ and W), secondary voids (f_s) and hardening (σ_0). The rates of the ligament parameter $\dot\chi$ and the void aspect ratio $\dot W$ read

$$\dot\chi = \frac{\dot R}{L}, \qquad \dot W = \frac{\dot h R - \dot R h}{R^2}, \tag{23}$$

where $\dot R$ and $\dot h$ are given by the trial velocity field (10). Since v_r depends on the variables r and z, it is necessary to consider some average value of it over the variable z so $\dot R$ is uniform; the following assumption is made:

$$\dot R \approx \frac{1}{h} \int_0^h v_r(R, z)\mathrm{d}z. \tag{24}$$

The evolution equations pertaining to primary voids are thus given by

$$\dot\chi = \frac{(1-\alpha_{\text{opt}})}{2}\left(\frac{1}{\chi} - \chi \right)\frac{D_{33}}{c}, \ \dot W = W\left(1 - \frac{(1-\alpha_{\text{opt}})}{2}\left(\frac{1}{\chi^2} - 1\right) \right)\frac{D_{33}}{c}. \tag{25}$$

The rate of the porosity of the second population $\dot f_s$ is obtained from the mass balance equation

$$\dot f_s = (1 - f_s)\text{tr}(\mathbf{d}), \tag{26}$$

where $\mathbf{d}$ is the strain rate associated with the trial velocity field (10). From equation (12), the mean strain rate is uniform in the ligament so the evolution equation pertaining to secondary voids is simply given by

$$\dot f_s = (1 - f_s)\alpha_{\text{opt}}\frac{D_{33}}{c}. \tag{27}$$

Finally, isotropic hardening is accounted for following Gurson (1977)'s classical heuristic approach. The yield limit σ_0 is replaced in the criterion by some "average yield stress" $\bar\sigma$ given by

$$\bar\sigma \equiv \sigma(\bar\varepsilon) \tag{28}$$

where $\sigma(\varepsilon)$ is a function providing the local yield limit as a function of the local cumulated plastic strain ε, and $\bar\varepsilon$ represents some "average equivalent strain" in the porous material. The evolution of $\bar\varepsilon$ is governed by the following equation:

$$(1 - c\chi^2)\bar\sigma\dot{\bar\varepsilon} = \Sigma_{33}D_{33}. \tag{29}$$

This equation expresses the heuristic assumption that the plastic dissipation in the heterogeneous porous material is equal to that in a fictitious "equivalent" homogeneous material with equivalent strain $\bar\varepsilon$ and yield stress $\bar\sigma$.

4. Numerical results

The aim of this section is to assess numerically the coalescence criterion derived in Section 3.

4.1. Description of the simulations

Numerical simulations are performed with the finite element method using an in-house code on 2D axymmetric meshes. Boundary conditions of type (1) are considered in order to impose coalescence. The limit-analysis problem is solved by considering an elastic-plastic evolution problem without any geometry update nor hardening, for which the limit-load is reached when the overall stress components no longer evolve (Michel et al., 1999). Two local behaviors are implemented; the model of Michel and Suquet (1992) is used in order to assess the model developed, and Gurson (1977)'s model is also considered to study the effect of the local potential (see Section 5.1). In both cases, a classical return-mapping algorithm is used to solve the local step (Simo and Taylor, 1986). The macroscopic limit-load Σ_{33} is calculated using the formula

$$\Sigma_{33} = \frac{1}{\text{vol}(\Omega)} \int_{\Omega - \omega} \sigma_{33} \, d\Omega. \tag{30}$$

In order to cover a large number of geometrical cases, a specific mesh generator has been developed. Eight-node quadratic elements subintegrated with 2×2 Gauss points are used. The mesh procedure, described in Appendix B, permits to obtain a total number of quadratic elements close to a prescribed value Q taken here as $Q = 5000$. This discretization is adequate for the numerical calculations envisaged, further mesh refinement making no appreciable difference to the results. For illustrative purpose, Fig. 3 shows the meshes used in the cases $W = 1$, $\chi = 0.2$, $c = 0.05$ and $W = 1$, $\chi = 0.7$, $c = 0.9$. The meshes contain respectively 5024 elements and 15,365 nodes (30,730 degrees of freedom) and 4767 elements and 14,766 nodes (29,532 degrees of freedom).

4.2. Influence of the parameter c

First, we study numerically the influence of the parameter $c = h/H$. Since the criterion for double porous materials (22) or any of the existing criteria for incompressible matrices (Benzerga and Leblond, 2014; Morin et al., 2015a; Hure and Barrioz, 2016) do not depend on this parameter, it is important to investigate numerically its effect and notably when it affects the limit-load of coalescence. The evolution of the axial stress Σ_{33} promoting coalescence is represented in Fig. 4 for $W = 1$.

The numerical simulations show that the parameter c has an influence only when it reaches important values (roughly $c > 0.5$) *and* when ligaments are thick (roughly $\chi < 0.4$). In this specific case, an increase of the parameter c, which corresponds to a decrease of the vertical ligament, results in a decrease of the limit-load: the deformation mechanism depends only on the value of the vertical spacing of the cavities. On the other hand, when those two conditions are not met, all the limit-loads coincide irrespective of the value of c, which means that the deformation mechanism does not depend on the vertical spacing of the cavities.

In order to complete these observations on deformation mechanisms, the distribution of the local plastic dissipation, defined by equation (16), is represented in Fig. 5 in the case $W = 1$, $\chi = 0.3$, $f_s = 10^{-5}$ and for two values of c, $c = 0.1$ or $c = 0.9$. When $c = 0.1$, the plastic dissipation localizes in the *horizontal ligament* between neighboring voids; this behavior is always observed for $c > 0.5$ irrespective of the value of χ and corresponds to the (classical) mode of coalescence by internal necking. When $c = 0.9$, the plastic dissipation localizes in the *vertical ligament* between neighboring voids; this behavior appears only for high values of c and low values of χ and corresponds to a mode of coalescence in columns (Gologanu et al., 2001), which is not the topic of this paper.

Consequently in the following, only low values of c will be considered in the comparisons in order to investigate solely coalescence by internal necking.
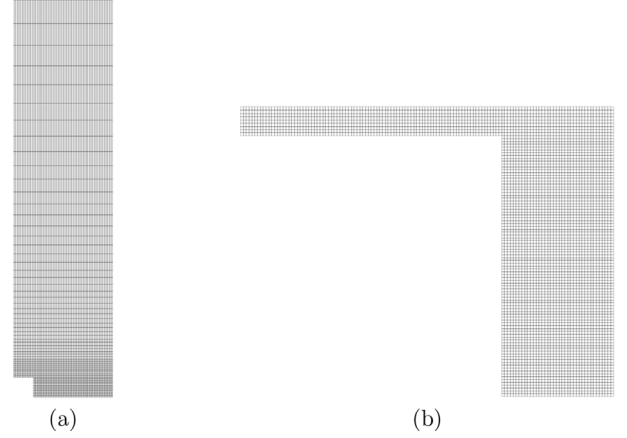

Fig. 3. Two examples of meshes used in the finite element calculations. Eight-node quadratic elements. (a) Mesh of the unit cell in the case $W = 1$, $\chi = 0.2$ and $c = 0.05$. (b) Mesh of the unit cell in the case $W = 1$, $\chi = 0.7$ and $c = 0.9$.

4.3. Study of coalescence by internal necking

We investigate now the comparison between model predictions and numerical simulations, only in the case of coalescence by internal necking; thus, the value $c = 0.1$ is considered in all the simulations. The limit-loads of coalescence are represented in Fig. 6 for various values of χ, W and f_s.

The main observation is that an increase of the second population porosity f_s results in a decrease of the limit-load promoting coalescence Σ_{33} for a given fixed primary cavity (corresponding to a couple W and χ), which is in general well reproduced by the model. In particular, a very good agreement is observed for elongated mesoscopic voids ($W = 2$) and all values of the porosity f_s. For flat mesoscopic voids ($W = 0.5$), the model tends to overestimate the limit-load when χ decreases, but only for low values of the porosity f_s. In this case, the model suffers from the exact same discrepancies than the "incompressible" model of Morin et al. (2015a) when $f_s = 0$, due to an inexact description of the distribution of the strain rate[1] (see Morin et al. (2015a)). The mediocre agreement observed in the incompressible case vanishes when f_s increases; an excellent agreement is even observed for $f_s = 10^{-1}$. It is also interesting to note that the presence of a second population "regularizes" to some extent the overall behavior: when $\chi \to 0$, the limit-load becomes finite if $f_s \neq 0$, in contrast with the infinite value observed for $f_s = 0$.

In order to understand more deeply the macroscopic results, the numerical velocity field is represented in some representative cases, in Fig. 7 for a small ligament parameter $\chi = 0.3$ and in Fig. 8 for a more important value $\chi = 0.6$. In each figure, the values $W = [0.5; 1; 2]$ and $f_s = [10^{-5}; 10^{-1}]$ are considered. The analytical velocity field is also represented for illustrative purpose in Fig. 9 for some values of the parameters.

The distribution of the numerical velocity field reveals two regimes of deformation: (i) a regime for which plastic flow is concentrated in both the horizontal and vertical ligaments. This happens only for small porosities f_s, flat primary cavities ($W < 1$) and small ligament parameters ($\chi \leq 0.4$). This has been already investigated for incompressible matrices (Morin et al., 2015a) and is confirmed here also for small second porosities f_s. (ii) A second regime is observed for which the plastic flow is concentrated only in the ligament between horizontal mesoscopic cavities. This takes place in the remaining geometrical cases considered and for all values of the second porosity. The analytical

---

[1] Note that it is possible to improve model's predictions for flat voids using a refined velocity field (Hure and Barrioz, 2016) or phenomenological modifications (Keralavarma and Chockalingam, 2016; Torki et al., 2017).
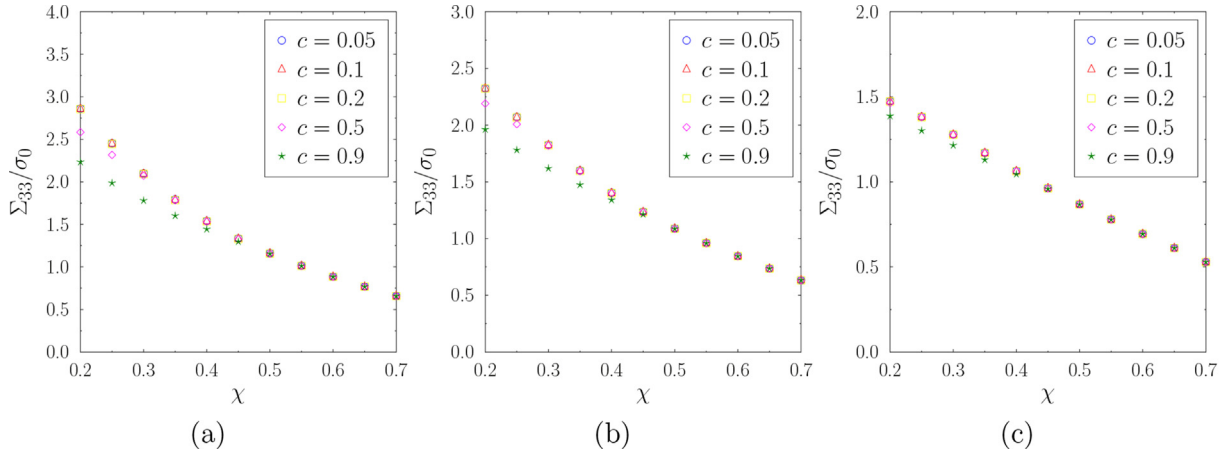
Fig. 4. Numerical results for the influence of the parameter c on the limit-load of coalescence for $W = 1$. (a) $f_s = 10^{-5}$, (b) $f_s = 10^{-2}$, (c) $f_s = 10^{-1}$.
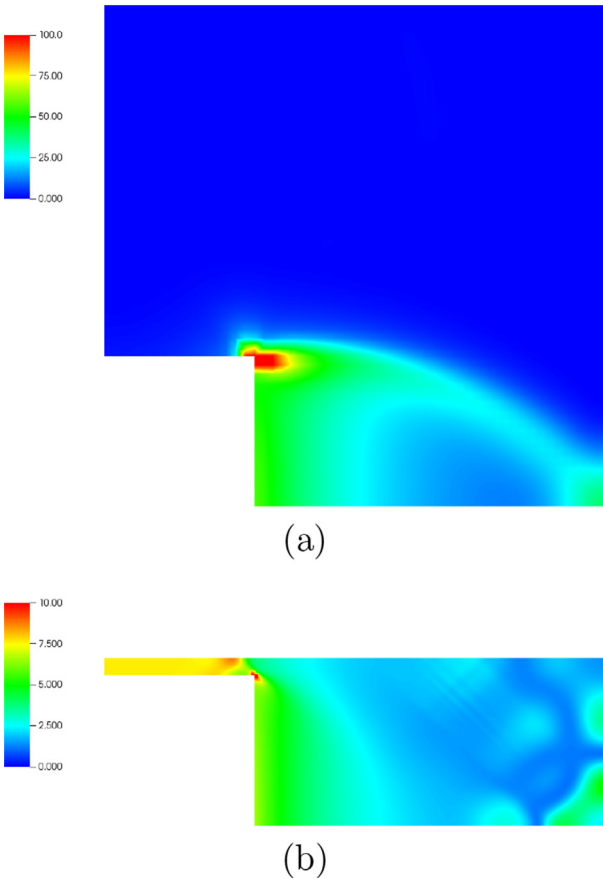

Fig. 5. Distribution of the numerical local plastic dissipation defined by equation (6) in the case $W = 1$, $\chi = 0.3$, $f_s = 10^{-5}$. (a) $c = 0.1$, (b) $c = 0.9$. Arbitrary units.

velocity field permits to reproduce quite accurately the second regime, which explains the relative good agreement between model's prediction and numerical results on the macroscopic limit-load in the geometric cases considered. In particular, this permits to explain why the model is not suitable for flat voids with a small and quasi-incompressible ligament (first regime), since plastic flow occurs in the vertical ligaments which is not taken into account by the model. However, when the second porosity increases (still in the same case of flat and small mesoscopic voids), the velocity field postulated in the model becomes very

close to the numerical one, resulting in a very good agreement of analytical and numerical limit-loads as shown in Fig. 6(a).

5. Discussion

5.1. Influence of the local potential

In the hypotheses made in the derivation of the model, the model of Michel and Suquet (1992) has been chosen to describe the second population of cavities. The choice of this microscopic potential over classical Gurson (1977)'s model was justified by the fact that it is more convenient to integrate in the calculation of the macroscopic plastic dissipation (16). If it seems a very hard task to derive a semi-analytical model with Gurson (1977)'s model in the matrix, it is however possible to investigate the overall behavior with the numerical micromechanical framework expounded in Section 4.1. Thus, the aim of this section is to study numerically the influence of the local porous potential on the macroscopic response of the double porous material. The numerical limit-loads of coalescence are represented in Fig. 10 in the case of a mesoscopic void with $W = 1$ and various porosities of the second population f_s, for Michel and Suquet (1992) and Gurson (1977)'s models.

It is interesting to note that the main differences appear for the intermediate value of the second population porosity $f_s = 10^{-2}$. This can be qualitatively interpreted by studying the two other asymptotic cases. When $f_s \rightarrow 0$, the two models of plastic porous materials reduce to an incompressible von Mises material and then yield to the same results. The differences between the two models are thus quite small for $f_s = 10^{-5}$. On the other hand, when $f_s \rightarrow 1$, the ligament becomes highly porous and the local stress triaxiality becomes important. In this case, the plastic potential of Gurson (1977) and Michel and Suquet (1992) becomes again very close since they both predict the same behavior at high triaxiality. Thus the predictions are very close for $f_s = 10^{-1}$. Consequently, only intermediate cases of moderate second porosity f_s will lead to (slightly) different results on the limit-loads for the double porous materials. Thus it appears that the choice of Michel and Suquet (1992)'s potential for the second population of cavities is a reasonable choice since it leads to very similar results than Gurson (1977)'s model.

5.2. Comparison with the existing criterion of Fabregue and Pardoen (2008)

Finally, we compare the predictions of the model developed with the existing criterion of Fabregue and Pardoen (2008, 2009). This model consists in a phenomenological extension of Thomason (1985)'s
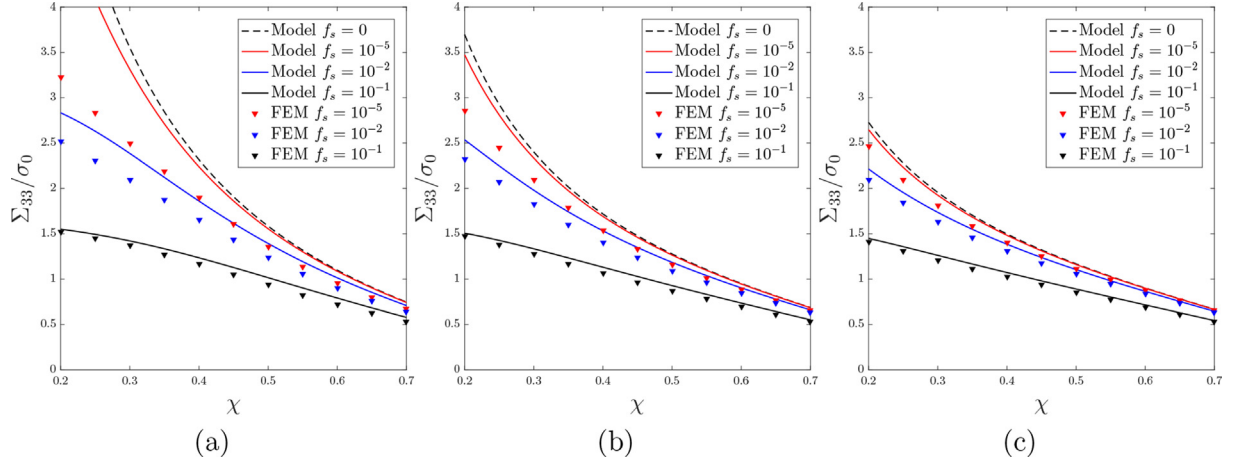
Fig. 6. Theoretical and numerical limit-loads of coalescence for various values of χ and f_s. (a) $W = 0.5$ (flat primary voids), (b) $W = 1$, (c) $W = 2$ (elongated primary voids).
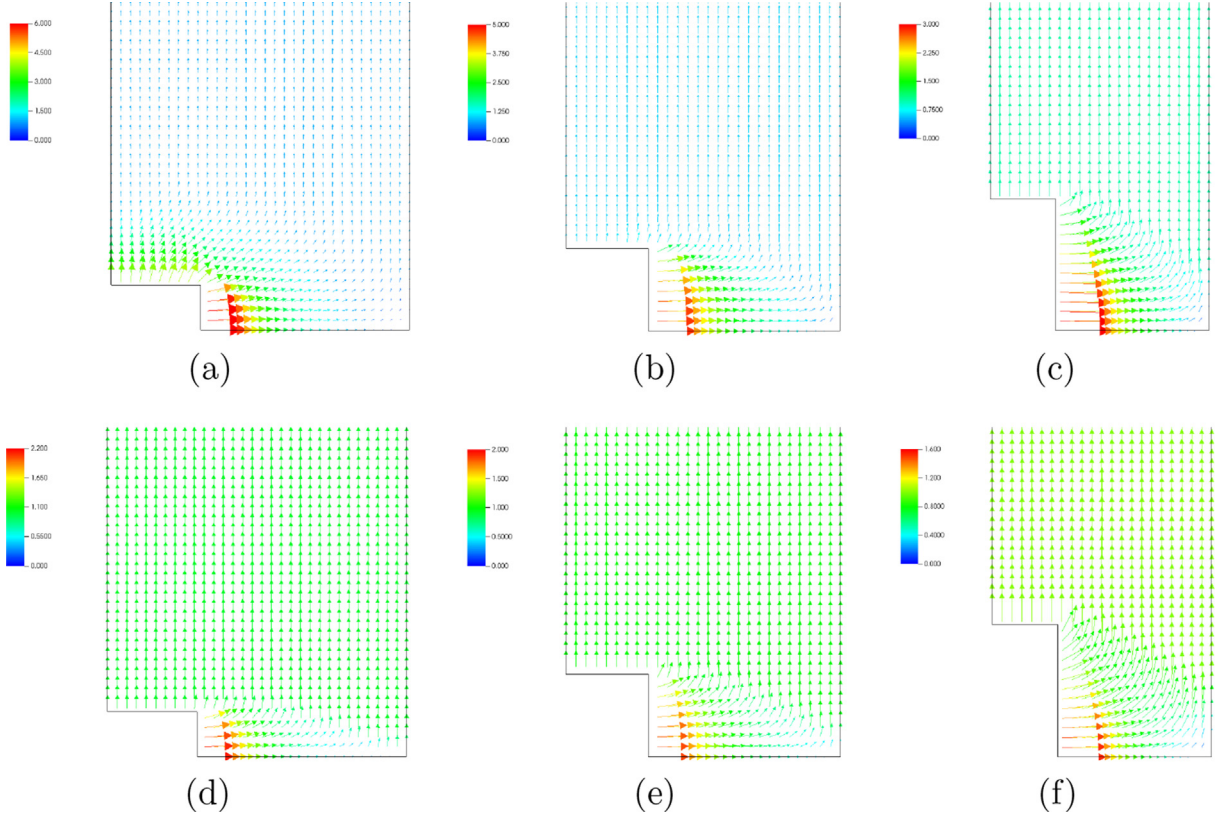

Fig. 7. Distribution of the numerical velocity field for a small ligament parameter $\chi = 0.3$. (a) $f_s = 10^{-5}$ and $W = 0.5$, (b) $f_s = 10^{-5}$ and $W = 1$, (c) $f_s = 10^{-5}$ and $W = 2$, (d) $f_s = 10^{-1}$ and $W = 0.5$, (e) $f_s = 10^{-1}$ and $W = 1$, (f) $f_s = 10^{-1}$ and $W = 2$. Arbitrary units.

criterion given by

$$\Phi^{FP}(\Sigma; \chi, W, f_s) = \frac{|\Sigma_{33}|}{\sigma_0} - (1 - f_s)(1 - \chi^2)\left[0.1\left(\frac{1 - \chi}{\chi W}\right)^2 + 1.24\sqrt{\frac{1}{\chi}}\right]$$

$$\leq 0, \qquad (31)$$

where the parameters χ and W are that defined in Section 2. It should be noted that, in this model, f_s was adjusted using micromechanical finite elements simulations in which the porosity of secondary voids was local. Two definitions for f_s were proposed, (i) as the mean value over the ligament and (ii) as the maximum value over the ligament,

which gave the best results. Despite the fact that the meaning of f_s in Fabregue and Pardoen (2008)'s model is not the same than that of the present model developed, both models are ultimately intended to describe the effect of secondary voids through their volume fraction. Consequently, it seems natural to compare both models for the same value f_s. Comparisons between the predictions of Fabregue and Pardoen (2008, 2009)'s model and that developed in Section 3 are thus provided for the same microstructural parameters in Fig. 11.

The model of Fabregue and Pardoen (2008) gives qualitatively a similar behavior than that developed in this work, namely a decrease of the limit-load of coalescence when the porosity of the second
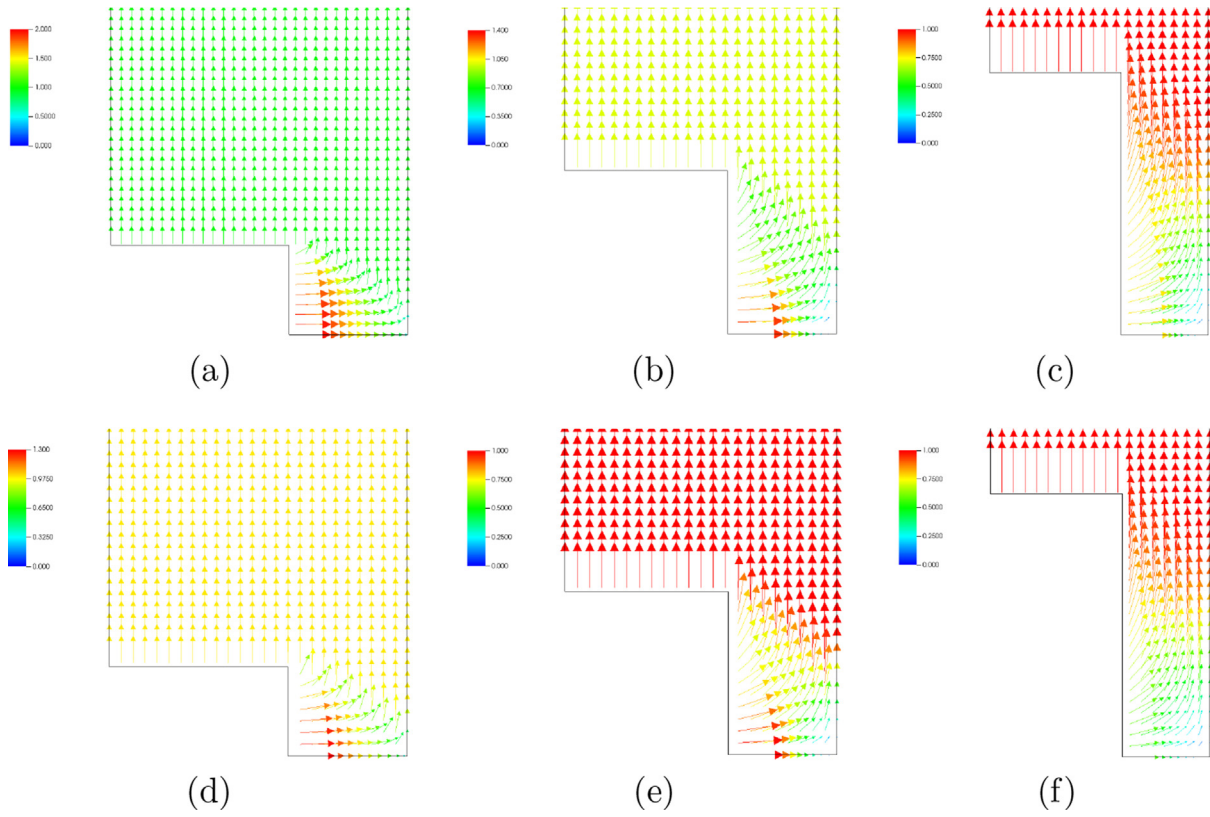
Fig. 8. Distribution of the numerical velocity field for a moderate ligament parameter $\chi = 0.6$. (a) $f_s = 10^{-5}$ and $W = 0.5$, (b) $f_s = 10^{-5}$ and $W = 1$, (c) $f_s = 10^{-5}$ and $W = 2$, (d) $f_s = 10^{-1}$ and $W = 0.5$, (e) $f_s = 10^{-1}$ and $W = 1$, (f) $f_s = 10^{-1}$ and $W = 2$. Arbitrary units.

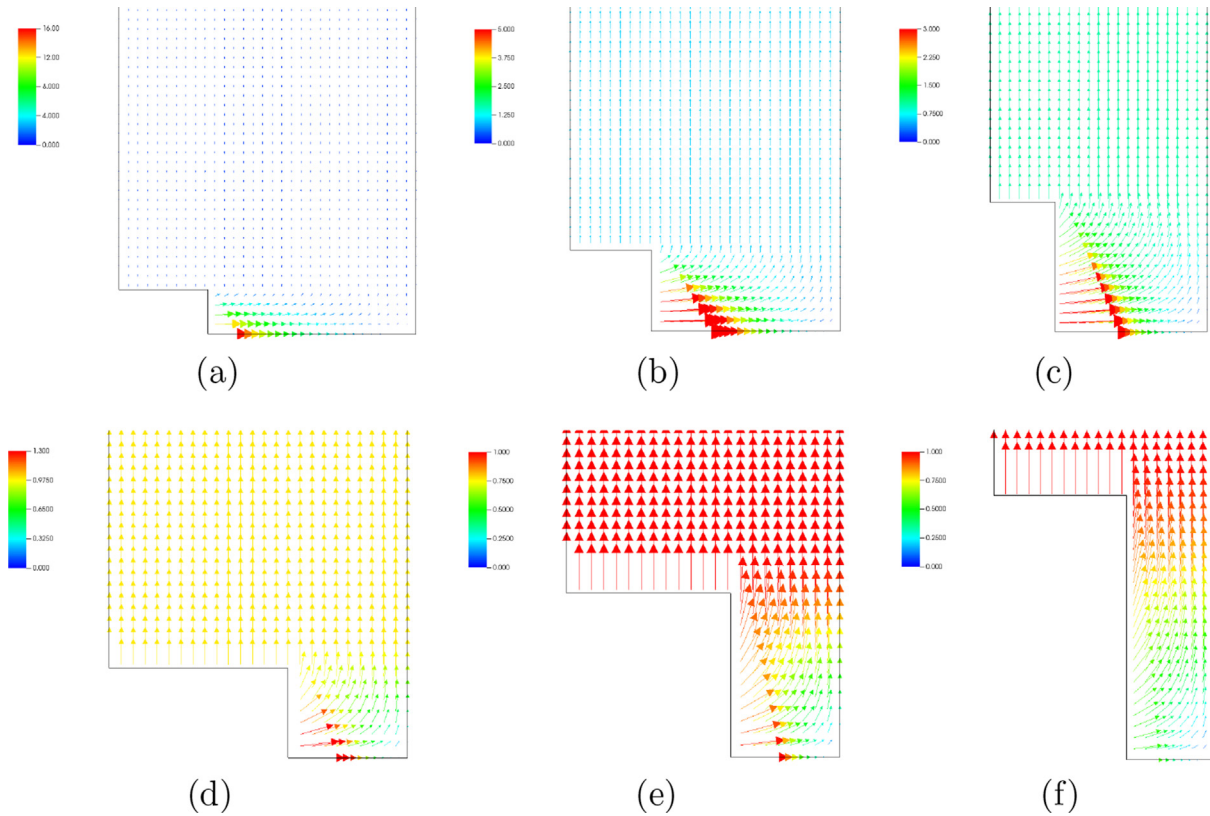**Fig. 9.** Distribution of the analytical velocity field. (a) $f_s = 10^{-5}$, $\chi = 0.3$ and $W = 0.5$, (b) $f_s = 10^{-5}$, $\chi = 0.3$ and $W = 1$, (c) $f_s = 10^{-5}$, $\chi = 0.3$ and $W = 2$, (d) $f_s = 10^{-1}$, $\chi = 0.6$ and $W = 0.5$, (e) $f_s = 10^{-1}$, $\chi = 0.6$ and $W = 1$, (f) $f_s = 10^{-1}$, $\chi = 0.6$ and $W = 2$. Arbitrary units.
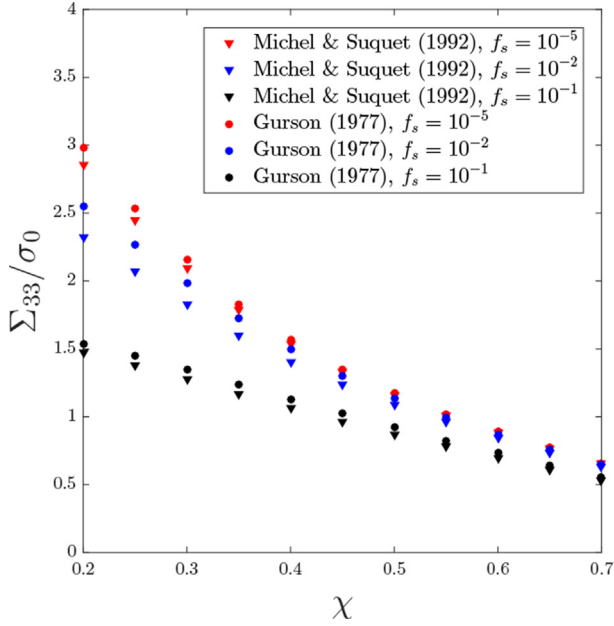
Fig. 10. Comparison between the numerical limit-loads of coalescence using Gurson (1977) and Michel and Suquet (1992) plastic potentials, for $W = 1$ and various values of χ and f_s.

population of cavities increases. However, the limit-load predicted by Fabregue and Pardoen (2008) is almost always higher, which means that it provides less accurate results since, from the theory of limit-analysis, the lowest limit-load provides the best results. Furthermore it should be noted that in the limit $\chi \to 0$ their model diverges like $1/\chi^2$ even for non-zero values of the porosity of the second population of cavities, which is not in agreement with the numerical results. However it should be noted that this model presents the advantage of being completely analytical.

6. Conclusion

The aim of this work was to derive a micromechanical criterion accounting for the presence of secondary cavities on the coalescence of primary voids. This was done by extending Benzerga and Leblond (2014) and Morin et al. (2015a)'s approach of coalescence by internal necking considering Michel and Suquet (1992)'s plastic potential for

porous materials in the matrix surrounding primary voids. The compressibility of the matrix was introduced through a scalar parameter in the trial velocity field, permitting to minimize the macroscopic plastic dissipation. The model derived, involving the presence of integrals needing a computational evaluation, has permitted to account micromechanically for the presence of the second population. The model was then assessed numerically using finite element simulations performed on the same cell than the analytical model. In general, the predictions of the model are in a very good agreement with the numerical results. In particular the model permits to reproduce the decrease of the limit-load promoting coalescence when the porosity of the second population of cavities increases, emphasizing that the model is suitable to describe the reduction of ductility observed in double porous materials.

The present study permits to quantify the influence of the secondary population on the onset of coalescence of primary voids. In particular, its effect is quite small for typical values of the internal parameters (basically $W > 1$, $0.3 < \chi < 0.4$ and $f_s > 10^{-3}$), emphasizing that simpler models (see e.g. Thomason (1985); Benzerga and Leblond (2010); Morin et al. (2015a); Hure and Barrioz (2016)), which do not account for a second population, are suitable when the porosity f_s is quite small. However, the present study also point out that the effect of f_s cannot be neglected when it reaches large values, as observed in polycristalline UO_2 (Vincent et al., 2009b, 2014b).

In order to improve the modeling of ductile materials involving separate populations of cavities, several directions can be explored:

- A future important work consists in investigating the predictions of the model on actual evolution problems. The comparison between model's predictions and the simulations of Fabregue and Pardoen (2008) will be decisive in order to assess the ability of the model to capture the loss of ductility due to the presence of secondary voids.
- In practice, ductile failure often occurs under combined tension and shear conditions. The influence of the shear stress on coalescence by internal necking has been recently tackled by Torki et al. (2015, 2017) in the case of incompressible materials. It could be interesting to extend their work to compressible materials in order to reproduce the reduction of ductility observed in the numerical simulations of Nielsen and Tvergaard (2011) on metallic materials containing two populations of cavities subjected to intense shearing.
- Size effects are expected to enhance the ductility of metals when cavities are very small, which can be the case for the second population. The effects of void size have been theoretically investigated on the growth (Dormieux and Kondo, 2010) and coalescence (Gallican and Hure, 2017) of primary nanoscopic voids, but
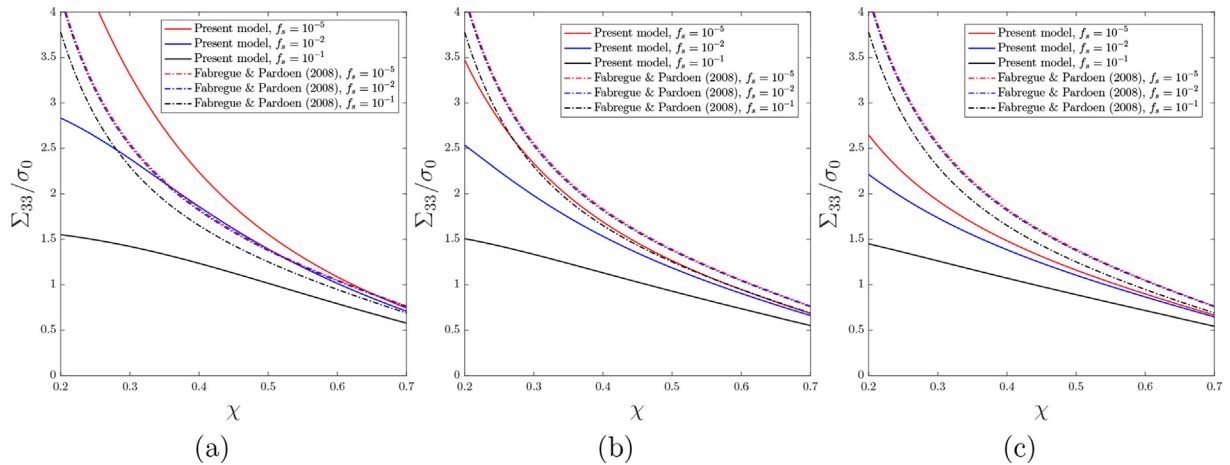

Fig. 11. Comparison between the predictions of the present model and that of Fabregue and Pardoen (2008) for various values of χ and f_s. (a) $W = 0.5$ (flat primary voids), (b) $W = 1$, (c) $W = 2$ (elongated primary voids).

their effects on secondary voids has only been studied numerically (Zybell et al., 2014). An extension to the present model to nanoscopic secondary voids could be interested to model nuclear fuel showing secondary voids of nanometer size (Dubourg et al., 2005).
- The distribution of the second population of cavities and the yield limit was supposed to be uniform in the present work. In order to provide a better description of the local fields, it would be interesting to consider an heterogeneous distribution of the second population of cavities and hardening, using the framework of sequential limit-analysis (Morin et al., 2017; Leblond et al., 2018).

A. Tabulated values for the optimal parameter α_{opt}

Values of the optimal parameter α_{opt} in the case $f_s = 10^{-1}$.

W \ χ	0.25	0.3	0.35	0.4	0.45	0.5	0.55	0.6	0.65	0.7
0.25	0.979	0.962	0.938	0.904	0.857	0.797	0.725	0.643	0.557	0.472
0.5	0.926	0.878	0.816	0.743	0.664	0.585	0.51	0.44	0.378	0.324
0.75	0.866	0.794	0.714	0.632	0.555	0.485	0.422	0.367	0.32	0.279
1	0.812	0.728	0.645	0.566	0.496	0.434	0.38	0.333	0.293	0.26
1.25	0.768	0.681	0.599	0.525	0.461	0.404	0.356	0.314	0.279	0.249
1.5	0.735	0.648	0.569	0.499	0.438	0.386	0.341	0.303	0.27	0.243
1.75	0.709	0.623	0.547	0.481	0.423	0.374	0.332	0.296	0.265	0.239
2	0.689	0.605	0.531	0.468	0.413	0.365	0.325	0.291	0.261	0.236
2.25	0.674	0.592	0.52	0.458	0.405	0.359	0.32	0.287	0.258	0.234
2.5	0.662	0.581	0.511	0.451	0.399	0.355	0.317	0.284	0.257	0.233

Values of the optimal parameter α_{opt} in the case $f_s = 10^{-2}$.

W \ χ	0.25	0.3	0.35	0.4	0.45	0.5	0.55	0.6	0.65	0.7
0.25	0.929	0.877	0.804	0.713	0.609	0.504	0.406	0.322	0.251	0.195
0.5	0.761	0.64	0.521	0.418	0.334	0.267	0.214	0.172	0.14	0.114
0.75	0.602	0.476	0.376	0.299	0.24	0.195	0.16	0.132	0.11	0.092
1	0.493	0.384	0.304	0.244	0.199	0.164	0.136	0.114	0.097	0.082
1.25	0.424	0.331	0.264	0.214	0.176	0.146	0.123	0.104	0.089	0.077
1.5	0.379	0.298	0.239	0.195	0.162	0.136	0.115	0.098	0.085	0.074
1.75	0.348	0.275	0.222	0.183	0.153	0.129	0.11	0.094	0.082	0.072
2	0.326	0.259	0.21	0.174	0.146	0.124	0.106	0.091	0.08	0.07
2.25	0.309	0.247	0.202	0.168	0.141	0.12	0.103	0.089	0.078	0.069
2.5	0.296	0.238	0.195	0.163	0.137	0.117	0.101	0.088	0.077	0.068

Values of the optimal parameter α_{opt} in the case $f_s = 10^{-3}$.

W \ χ	0.25	0.3	0.35	0.4	0.45	0.5	0.55	0.6	0.65	0.7
0.25	0.841	0.737	0.612	0.486	0.373	0.283	0.214	0.161	0.122	0.092
0.5	0.536	0.394	0.291	0.218	0.166	0.128	0.101	0.08	0.064	0.051
0.75	0.351	0.253	0.189	0.144	0.113	0.09	0.073	0.059	0.049	0.041
1	0.262	0.192	0.146	0.114	0.091	0.074	0.061	0.051	0.042	0.036
1.25	0.214	0.159	0.123	0.098	0.079	0.065	0.054	0.046	0.039	0.033
1.5	0.185	0.14	0.11	0.088	0.072	0.06	0.05	0.043	0.037	0.031
1.75	0.166	0.127	0.101	0.082	0.067	0.056	0.048	0.041	0.035	0.03
2	0.153	0.118	0.094	0.077	0.064	0.054	0.046	0.039	0.034	0.029
2.25	0.143	0.112	0.09	0.074	0.061	0.052	0.044	0.038	0.033	0.029
2.5	0.136	0.107	0.086	0.071	0.059	0.05	0.043	0.037	0.032	0.028

Values of the optimal parameter α_{opt} in the case $f_s = 10^{-4}$.

W \ χ	0.25	0.3	0.35	0.4	0.45	0.5	0.55	0.6	0.65	0.7
0.25	0.725	0.576	0.432	0.315	0.229	0.168	0.124	0.092	0.069	0.051
0.5	0.351	0.24	0.17	0.125	0.094	0.072	0.056	0.044	0.035	0.028
0.75	0.208	0.145	0.107	0.081	0.063	0.05	0.04	0.033	0.027	0.022
1	0.15	0.108	0.081	0.063	0.05	0.041	0.033	0.028	0.023	0.02
1.25	0.12	0.089	0.068	0.054	0.044	0.036	0.03	0.025	0.021	0.018
1.5	0.103	0.077	0.06	0.048	0.039	0.033	0.027	0.023	0.02	0.017
1.75	0.092	0.07	0.055	0.045	0.037	0.031	0.026	0.022	0.019	0.016
2	0.084	0.065	0.051	0.042	0.035	0.029	0.025	0.021	0.018	0.016
2.25	0.078	0.061	0.049	0.04	0.033	0.028	0.024	0.02	0.018	0.015
2.5	0.074	0.058	0.047	0.038	0.032	0.027	0.023	0.02	0.017	0.015

Values of the optimal parameter α_{opt} in the case $f_s = 10^{-5}$.

W \ χ	0.25	0.3	0.35	0.4	0.45	0.5	0.55	0.6	0.65	0.7
0.25	0.596	0.431	0.3	0.21	0.149	0.108	0.079	0.059	0.044	0.033
0.5	0.233	0.155	0.109	0.079	0.06	0.046	0.036	0.028	0.022	0.018
0.75	0.133	0.092	0.067	0.051	0.04	0.031	0.025	0.021	0.017	0.014
1	0.094	0.068	0.051	0.04	0.032	0.026	0.021	0.017	0.015	0.012
1.25	0.075	0.055	0.043	0.034	0.027	0.022	0.019	0.016	0.013	0.011
1.5	0.064	0.048	0.038	0.03	0.025	0.02	0.017	0.014	0.012	0.011
1.75	0.057	0.043	0.034	0.028	0.023	0.019	0.016	0.014	0.012	0.01
2	0.052	0.04	0.032	0.026	0.022	0.018	0.015	0.013	0.011	0.01
2.25	0.049	0.038	0.03	0.025	0.021	0.017	0.015	0.013	0.011	0.01
2.5	0.046	0.036	0.029	0.024	0.02	0.017	0.014	0.012	0.011	0.009

B. Mesh procedure

The geometry of the unit cell is entirely determined by the triplet (W, χ, c). The mesh procedure is given by the following steps:

1. The cell is divided in two parts: (i) the ligament $\Omega_{\text{lig}} - \omega$ ($R \leq r \leq L$, $0 \leq z \leq h$) is cut into $n \times m$ elements and (ii) the upper region $\Omega - \Omega_{\text{lig}}$ ($0 \leq r \leq L$, $h \leq z \leq H$) is cut into $k \times \ell$ elements.
2. The $n \times m$ elements in the ligament are taken identical as square elements with

$$n = \text{floor}(k(1 - \chi)), \quad m = \text{floor}(kW\chi), \tag{B.1}$$

where floor(x) is the classical floor function of x.

3. In order not to increase uselessly the number of elements when H is bigger than h, the position and size of the $k \times \ell$ elements in the upper region follows the geometric progression

$$z_j = h\,q^j, \quad q = c^{-\frac{1}{\ell}}, \quad j = 0, .., \ell, \tag{B.2}$$

where z_j denotes the axial position of element j. We impose that the height of the first row of elements has a similar size than the elements of the ligament; ℓ is then taken equal to

$$\ell = \text{floor}\left(\ln\left(\frac{1}{c}\right)/\ln\left(1 + \frac{1}{kW\chi}\right)\right). \tag{B.3}$$

4. The desired total number of elements is denoted Q; in order to satisfy at best this objective, the number of elements k is taken equal to

$$k = \text{floor}(\sqrt{Q/(W\chi(1 - \chi - \ln(c)))}). \tag{B.4}$$

References

Benzerga, A.A., Leblond, J.B., 2010. Ductile fracture by void growth to coalescence. Adv. Appl. Mech. 44, 169–305.

Benzerga, A.A., Leblond, J.B., 2014. Effective yield criterion accounting for microvoid coalescence. J. Appl. Mech. 81, 031009.

Benzerga, A.A., Leblond, J.B., Needleman, A., Tvergaard, V., 2016. Ductile failure modeling. Int. J. Fract. 201, 29–80.

Boittin, G., Vincent, P.G., Moulinec, H., Garajeu, M., 2017. Numerical simulations and modeling of the effective plastic flow surface of a biporous material with pressurizedintergranular voids. Comput. Meth. Appl. Mech. Eng. 323, 174–201.

Cox, T.B., Low, J.R., 1974. An investigation of the plastic fracture of AISI 4340 and 18 Nickel-200 grade maraging steels. Metallurgical Transactions 5, 1457–1470.

Danas, K., Ponte Castaneda, P., 2009. A finite-strain model for anisotropic viscoplastic porous media: I Theory. Eur. J. Mech. Solid. 28, 387–401.

Dormieux, L., Kondo, D., 2010. An extension of Gurson model incorporating interface stresses effects. Int. J. Eng. Sci. 48, 575–581.

Dubourg, R., Faure-Geors, H., Nicaise, G., Barrachin, M., 2005. Fission product release in the first two PHEBUS tests FPT0 and FPT1. Nucl. Eng. Des. 235, 2183–2208.

Fabregue, D., Pardoen, T., 2008. A constitutive model for elastoplastic solids containing primary and secondary voids. J. Mech. Phys. Solid. 56, 719–741.

Fabregue, D., Pardoen, T., 2009. Corrigendum to A constitutive model for elastoplastic solids containing primary and secondary voids. [J. Mech. Phys. Solids 56 (2008) 719741]. J. Mech. Phys. Solid. 57, 869–870.

Faleskog, J., Shih, C.F., 1997. Micromechanics of coalescence–I. Synergistic effects of elasticity, plastic yielding and multi-size-scale voids. J. Mech. Phys. Solid. 45, 21–50.

Gallican, V., Hure, J., 2017. Anisotropic coalescence criterion for nanoporous materials. J. Mech. Phys. Solid. 108, 30–48.

Gologanu, M., Leblond, J.B., Devaux, J., 1993. Approximate models for ductile metals containing non-spherical voids–Case of axisymmetric prolate ellipsoidal cavities. J. Mech. Phys. Solid. 41, 1723–1754.

Gologanu, M., Leblond, J.B., Devaux, J., 2001. Theoretical models for void coalescence in porous ductile solids. II. Coalescence in columns. Int. J. Solid Struct. 38, 5595–5604.

Gurson, A.L., 1977. Continuum theory of ductile rupture by void nucleation and growth: Part I–Yield criteria and flow rules for porous ductile media. ASME Journal of Engineering Materials and Technology 99, 2–15.

Hure, J., Barrioz, P.O., 2016. Theoretical estimates for flat voids coalescence by internal necking. Eur. J. Mech. Solid. 60, 217–226.

Julien, J., Garajeu, M., Michel, J.C., 2011. A semi-analytical model for the behavior of saturated viscoplastic materials containing two populations of voids of different sizes. Int. J. Solid Struct. 48, 1485–1498.

Kailasam, M., Ponte Castaneda, P., 1998. A general constitutive theory for linear and nonlinear particulate media with microstructure evolution. J. Mech. Phys. Solid. 46, 427–465.

Keralavarma, S., Benzerga, A., 2010. A constitutive model for plastically anisotropic solids with non-spherical voids. J. Mech. Phys. Solid. 58, 874–901.

Keralavarma, S.M., 2017. A multi-surface plasticity model for ductile fracture simulations. J. Mech. Phys. Solid. 103, 100–120.

Keralavarma, S.M., Chockalingam, S., 2016. A criterion for void coalescence in anisotropic ductile materials. Int. J. Plast. 82, 159–176.

Khan, I.A., Bhasin, V., 2017. On the role of secondary voids and their distribution in the mechanism of void growth and coalescence in porous plastic solids. Int. J. Solid Struct. 108, 203–215.

Khdir, Y.K., Kanit, T., Zari, F., Nat-Abdelaziz, M., 2014. Computational homogenization of plastic porous media with two populations of voids. Mater. Sci. Eng. 597, 324–330.

Koplik, J., Needleman, A., 1988. Void growth and coalescence in porous plastic solids. Int. J. Solid Struct. 24, 835–853.

Leblond, J., Kondo, D., Morin, L., Remmal, A., 2018. Classical and sequential limit-analysis revisited. Compt. Rendus Mec. 346, 336–349.

Leblond, J., Perrin, G., Devaux, J., 1995. An improved Gurson-type model for hardenable ductile metals. Eur. J. Mech. Solid. 14, 499–527.

Madou, K., Leblond, J.B., 2012. A Gurson-type criterion for porous ductile solids containing arbitrary ellipsoidal cavities–I: limit-analysis of some representative cell. J. Mech. Phys. Solid. 60, 1020–1036.

Marini, B., Mudry, F., Pineau, A., 1985. Experimental study of cavity growth in ductile rupture. Eng. Fract. Mech. 22, 989–996.

Michel, J.C., Moulinec, H., Suquet, P., 1999. Effective properties of composite materials with periodic microstructure: a computational approach. Comput. Meth. Appl. Mech. Eng. 172, 109–143.

Michel, J.C., Suquet, P., 1992. The constitutive law of nonlinear viscous and porous materials. J. Mech. Phys. Solid. 40, 783–812.

Monchiet, V., Cazacu, O., Charkaluk, E., Kondo, D., 2008. Macroscopic yield criteria for plastic anisotropic materials containing spheroidal voids. Int. J. Plast. 24, 1158–1189.

Morin, L., Leblond, J.B., Benzerga, A.A., 2015a. Coalescence of voids by internal necking: theoretical estimates and numerical results. J. Mech. Phys. Solid. 75, 140–158.

Morin, L., Leblond, J.B., Benzerga, A.A., Kondo, D., 2016. A unified criterion for the growth and coalescence of microvoids. J. Mech. Phys. Solid. 97, 19–36.

Morin, L., Leblond, J.B., Kondo, D., 2015b. A Gurson-type criterion for plastically anisotropic solids containing arbitrary ellipsoidal voids. Int. J. Solid Struct. 77, 86–101.

Morin, L., Michel, J.C., Leblond, J.B., 2017. A Gurson-type layer model for ductile porous solids with isotropic and kinematic hardening. Int. J. Solid Struct. 118, 167–178.

Nielsen, K.L., Tvergaard, V., 2011. Failure by void coalescence in metallic materials containing primary and secondary voids subject to intense shearing. Int. J. Solid Struct. 48, 1255–1267.

Perrin, G., Leblond, J.B., 1990. Analytical study of a hollow sphere made of plastic porous material and subjected to hydrostatic tension–Application to some problems in ductile fracture of metals. Int. J. Plast. 6, 677–699.

Perrin, G., Leblond, J.B., 2000. Accelerated void growth in porous ductile solids containing two populations of cavities. Int. J. Plast. 16, 91–120.

Pineau, A., Benzerga, A.A., Pardoen, T., 2016. Failure of metals I: brittle and ductile fracture. Acta Mater. 107, 424–483.

Ponte Castaneda, P., 1991. The effective mechanical properties of nonlinear isotropic composites. J. Mech. Phys. Solid. 39, 45–71.

Shen, W.Q., Shao, J.F., Dormieux, L., Kondo, D., 2012. Approximate criteria for ductile porous materials having a Green type matrix: application to double porous media. Comput. Mater. Sci. 62, 189–194.

Shen, W.Q., Shao, J.F., Kondo, D., 2017. Macroscopic criteria for Green type porous materials with spheroidal voids: application to double porous materials. Int. J. Numer. Anal. Meth. GeoMech. 41, 1453–1473.

Simo, J.C., Taylor, R.L., 1986. A return mapping algorithm for plane stress elastoplasticity. Int. J. Numer. Meth. Eng. 22, 649–670.

Tekoglu, C., 2015. Void coalescence in ductile solids containing two populations of voids. Eng. Fract. Mech. 147, 418–430.

Thomason, P.F., 1985. A three-dimensional model for ductile fracture by the growth and coalescence of microvoids. Acta Metall. 33, 1087–1095.

Torki, M.E., Benzerga, A.A., Leblond, J.B., 2015. On void coalescence under combined tension and shear. J. Appl. Mech. 82, 071005.

Torki, M.E., Tekoglu, C., Leblond, J.B., Benzerga, A.A., 2017. Theoretical and numerical analysis of void coalescence in porous ductile solids under arbitrary loadings. Int. J. Plast. 91, 160–181.

Tvergaard, V., Needleman, A., 1984. Analysis of the cup-cone fracture in a round tensile bar. Acta Metall. 32, 157–169.

Vincent, P.G., Monerie, Y., Suquet, P., 2009a. Porous materials with two populations of voids under internal pressure: I. Instantaneous constitutive relations. Int. J. Solid Struct. 46, 480–506.

Vincent, P.G., Monerie, Y., Suquet, P., 2009b. Porous materials with two populations of voids under internal pressure: II. Growth and coalescence of voids. Int. J. Solid Struct. 46, 507–526.

Vincent, P.G., Suquet, P., Monerie, Y., Moulinec, H., 2014a. Effective flow surface of porous materials with two populations of voids under internal pressure: I. A GTN model. Int. J. Plast. 56, 45–73.

Vincent, P.G., Suquet, P., Monerie, Y., Moulinec, H., 2014b. Effective flow surface of porous materials with two populations of voids under internal pressure: II. Full-field simulations. Int. J. Plast. 56, 74–98.

Willis, J.R., 1991. On methods for bounding the overall properties of nonlinear composites. J. Mech. Phys. Solid. 39, 73–86.

Zybell, L., Hutter, G., Linse, T., Muhlich, U., Kuna, M., 2014. Size effects in ductile failure of porous materials containing two populations of voids. Eur. J. Mech. Solid. 45, 8–19.